

# Electrical resistivity anomaly, valence shift of Pr ion, and magnetic behavior in epitaxial $(\text{Pr}_{1-y}\text{Y}_y)_{1-x}\text{Ca}_x\text{CoO}_3$ thin films under compressive strain

H. Fujishiro, Y. Noda, K. Akuzawa, T. Naito, A. Ito, T. Goto, M. Marysko, Z. Jirak, J. Hejtmanek, and K. Nitta

Citation: *Journal of Applied Physics* **121**, 115104 (2017); doi: 10.1063/1.4978747

View online: <http://dx.doi.org/10.1063/1.4978747>

View Table of Contents: <http://aip.scitation.org/toc/jap/121/11>

Published by the *American Institute of Physics*

---

---



Small Conferences. BIG Ideas.

Applied Physics  
Reviews

SAVE THE DATE!  
**3D Bioprinting: Physical and Chemical Processes**  
May 2–3, 2017 • Winston Salem, NC, USA

The background of the banner features a stylized, glowing blue and red network of lines, resembling a biological or chemical structure, set against a dark blue background.

# Electrical resistivity anomaly, valence shift of Pr ion, and magnetic behavior in epitaxial $(\text{Pr}_{1-y}\text{Y}_y)_{1-x}\text{Ca}_x\text{CoO}_3$ thin films under compressive strain

H. Fujishiro,<sup>1,a)</sup> Y. Noda,<sup>1</sup> K. Akuzawa,<sup>1</sup> T. Naito,<sup>1</sup> A. Ito,<sup>2,3</sup> T. Goto,<sup>2</sup> M. Marysko,<sup>4</sup> Z. Jirak,<sup>4</sup> J. Hejtmánek,<sup>4</sup> and K. Nitta<sup>5</sup>

<sup>1</sup>Faculty of Science and Engineering, Iwate University, 4-3-5 Ueda, Morioka 020-8551, Japan

<sup>2</sup>Institute for Materials Research, Tohoku University, 2-1-1 Katahira, Sendai 980-8577, Japan

<sup>3</sup>Graduate School of Environment and Information Sciences, Yokohama National University, 79-7 Tokiwadai, Yokohama 240-8501, Japan

<sup>4</sup>Institute of Physics, ASCR, Cukrovarnicka 10, 162 00 Prague 6, Czech Republic

<sup>5</sup>Japan Synchrotron Radiation Research Institute, SPring-8, 1-1-1 Kouto, Sayo 679-5198, Japan

(Received 22 October 2016; accepted 4 March 2017; published online 21 March 2017)

We have fabricated  $(\text{Pr}_{1-y}\text{Y}_y)_{1-x}\text{Ca}_x\text{CoO}_3$  (PYCCO) epitaxial films with various thicknesses by pulsed laser deposition on the  $\text{SrLaAlO}_4$  (SLAO) substrate that applied an in-plane compressive stress to the film, and investigated the temperature dependence of the electrical resistivity,  $\rho(T)$ , of the films. An anomalous  $\rho(T)$  upturn with a broad hysteresis could be clearly observed only for the thinnest film ( $d = 50$  nm), and the  $\rho(T)$  anomaly decreased by increasing film thickness,  $d$ . The temperature dependence of the X-ray absorption near-edge structure (XANES) spectra at Pr  $L_2$ -edge was measured for the films, and the valence states of praseodymium (Pr) ion were determined using the analysis of the XANES spectra. As a result, the average valence of the Pr ion in the  $d = 50$  nm film slightly increases with decreasing temperature from the common value of 3.0+ around room temperature to 3.15+ at 8 K. The valence shift of Pr is thus similar to what was observed on the PYCCO polycrystalline bulks with an abrupt metal-insulator transition, accompanied by a spin-state (SS) transition of Co ions. Furthermore, the low-temperature SQUID measurements evidenced a paramagnetic behavior down to the lowest temperature, which suggests that the dominant part of  $\text{Co}^{3+}$  ions in the film grown on the SLAO substrate tends to be in the low spin state characteristic for the insulating ground state. These results strongly suggest that the anomalous  $\rho(T)$  upturn in the thin films on the  $\text{SrLaAlO}_4$  (SLAO) substrate is closely related to the SS transition of Co ions. On the other hand, PYCCO films grown on the  $\text{LaAlO}_3$  (LAO) substrate that applied an in-plane tensile stress showed no valence shift of Pr ions and developed a long range ferromagnetic order, which points to a complete suppression of the low-temperature transition. The behaviors of the epitaxial films are discussed in terms of the in-plane stress exerted by different substrates and accumulated elastic energy. *Published by AIP Publishing.* [<http://dx.doi.org/10.1063/1.4978747>]

## I. INTRODUCTION

Perovskite cobaltite  $\text{LaCoO}_3$  and its rare-earth analogs show marked evolutions of the electric and magnetic properties, which have a microscopic origin in the temperature-induced spin-state (SS) crossovers of the octahedrally coordinated  $\text{Co}^{3+}$  ions of  $3d^6$  electronic configuration.<sup>1-7</sup> The insulating ground state of these systems is based on  $\text{Co}^{3+}$  ions in the diamagnetic low spin state (LS;  $t_{2g}^6 e_g^0$ ,  $S = 0$ ), while a paramagnetic insulating phase is gradually formed by local excitation of higher spin states, which takes place in rather broad temperature interval (40–120 K for  $\text{LaCoO}_3$ ). The nature of such thermally activated species, the high spin (HS;  $t_{2g}^4 e_g^2$ ,  $S = 2$ ) or intermediate spin (IS;  $t_{2g}^5 e_g^1$ ,  $S = 1$ )  $\text{Co}^{3+}$  ions, was under a long-time debate. The electromagnetic phase transition,<sup>8,9</sup> metal-insulator (MI) transition,<sup>10</sup> and the existence of various magnetic states, including ferromagnetic, cluster glass, and spin glass,<sup>11-13</sup> have been reported and discussed. Nonetheless, the recent experiments and electronic structure calculations are strongly in favor of

a mixed LS/HS phase, where HS sites experience mutual repulsions.<sup>14,15</sup> There is also large uncertainty about the transition to metallic phase at high temperatures ( $\sim 500$  K for  $\text{LaCoO}_3$ ). While the paramagnetic susceptibility has been found to be close to what is expected for homogeneous IS phase (cobalt ions in  $t_{2g}^5 \sigma^*$  state),<sup>16</sup> there is a growing evidence for a more complex disproportionation involving all the three states (LS, IS, and HS), which is controlled not only by the delicate balance of local energy terms (crystal field splitting vs. Hund-rule coupling) but also by pair interactions between the local states (repulsive for HS and attractive for IS).<sup>14,17</sup> Theoretical analysis performed on the basis of extensive dynamical mean-field theory (DMFT) calculations provides some view of what happens in such dynamic coexistences—with increasing temperature, the HS states gain progressively more weight over the LS ones, and the IS states arise only as short-living fluctuations.<sup>15</sup>

The properties of mixed-valence cobaltites also attract a lot of interest. The divalent substitution for La or rare-earth site, in  $\text{La}_{1-x}\text{Sr}_x\text{CoO}_3$  for instance, dopes hole carriers into the system, which in turn results in stabilization of finite spin states, formation of ferromagnetic droplets, and a phase

<sup>a)</sup>E-mail: fujishiro@iwate-u.ac.jp

separated state of ferromagnetic cluster in a non-ferromagnetic matrix for  $0.04 < x < 0.22$ , and a ferromagnetic metal phase with itinerant cobalt states for  $x > 0.22$ .<sup>8</sup> Most interestingly, some (Pr,Ca)-based cobaltites exhibit a pronounced first-order transition to a low-temperature phase with a weakly paramagnetic character and reduced electrical conductivity. This effect was revealed for the first time on  $\text{Pr}_{0.5}\text{Ca}_{0.5}\text{CoO}_3$  at  $T_{\text{MI}} \sim 90$  K by a step-like resistivity jump and concomitant anomalies in magnetic susceptibility, heat capacity, lattice dilatation, and photoemission spectroscopy.<sup>18–20</sup> The mechanism of the transition was tentatively ascribed to a spin-state crossover from the itinerant cobalt states to an ordered mixture of localized LS  $\text{Co}^{3+}$  and LS  $\text{Co}^{4+}$  ( $t_{2g}^5 e_g^0$ ,  $S = 1/2$ ) states. The MI transition was also evidenced in the less-doped  $\text{Pr}_{1-x}\text{Ca}_x\text{CoO}_3$  ( $x = 0.3$ ) under higher hydrostatic pressures,<sup>21,22</sup> and in the  $(\text{Pr}_{1-y}\text{RE}_y)_{1-x}\text{Ca}_x\text{CoO}_3$  system ( $0.2 < x < 0.5$ ) with a partial substitution of Pr by smaller RE cations such as Sm, Eu, and Y under ambient pressure.<sup>22,23</sup> This peculiar transition appeared to be conditioned not only by the presence of both Pr and Ca ions, but also by a larger structural distortion of the  $\text{CoO}_6$  network, depending on the average ionic radius and the size mismatch of perovskite A-site ions.<sup>23</sup> Furthermore, the critical temperature,  $T_{\text{MI}}$ , was found to decrease in a magnetic field, and the transition could be completely suppressed in very high magnetic fields.<sup>24</sup>

An alternative scenario explaining the nature of such a specific transition was proposed on the basis of electronic structure calculations exploiting the temperature dependence of the structural experimental data for  $\text{Pr}_{0.5}\text{Ca}_{0.5}\text{CoO}_3$ .<sup>25</sup> The calculations suggested that the formal cobalt valence would change below  $T_{\text{MI}}$  from a mixed-valence  $\text{Co}^{3.5+}$  towards a pure  $\text{Co}^{3.0+}$  with a strong preference for the LS state and, concomitantly, the praseodymium valence would increase from  $\text{Pr}^{3+}$  towards  $\text{Pr}^{4+}$ . The theoretical hypothesis about the crucial role of variable praseodymium valence was experimentally supported by the observation of a Schottky peak in the low temperature specific heat of  $(\text{Pr}_{1-y}\text{Y}_y)_{0.7}\text{Ca}_{0.3}\text{CoO}_3$  ( $y = 0.075$  and  $0.15$ ),<sup>26</sup> by X-ray absorption near-edge structure (XANES) spectra directly at the Pr  $L_3$ -edge,<sup>27–30</sup> and by small-angle neutron scattering measurements.<sup>31</sup>

It is generally desirable to use a single crystal or an epitaxial film for the physical investigation. In the epitaxial thin film, the electrical conduction and the spin state change, which depend on the lattice mismatch between the cobaltite and the substrate, the film thickness, and the fabrication condition.<sup>32</sup> In particular, the interface between the film and the substrate can play an important role, giving rise to boundary regions with different structures and affecting the transport and magnetic properties due to the induced strain, especially in very thin films. The experiments on  $\text{LaCoO}_3$  epitaxial films have demonstrated very different behaviors for strained films grown on  $(\text{La,Sr})(\text{Al,Ta})\text{O}_3$  (LSAT) substrate, applying an in-plane tensile stress, and those grown on  $\text{LaAlO}_3$  (LAO) substrate, applying a compressive stress. In the latter case, a paramagnetic ground state is obtained, which may signal the dominance of LS cobalt species as in bulk  $\text{LaCoO}_3$ , whereas the tensile stress stabilizes long-range ferromagnetic order below  $\sim 85$  K.<sup>33</sup> In the case of thicker films ( $d > 50$  nm),

where epitaxial strain is relaxed to a high degree, the long-range ferromagnetic order is stabilized for the films grown both on the LAO and LSAT substrates.

As the  $(\text{Pr}_{1-y}\text{RE}_y)_{1-x}\text{Ca}_x\text{CoO}_3$  system is concerned, no single crystal sample was reported and all previous experimental studies of the simultaneous MI-SS transition have been performed on polycrystalline bulk materials. Only recently, we successfully fabricated  $(\text{Pr}_{1-y}\text{M}_y)_{1-x}\text{Ca}_x\text{CoO}_3$  epitaxial films ( $M = \text{Y, Gd}$ ) of 50 nm in thickness by pulsed laser deposition (PLD) on single crystal substrates with different lattice parameters, and measured their electrical resistivity,  $\rho(T)$ .<sup>34</sup> An anomalous  $\rho(T)$  upturn with a wide hysteresis can be clearly seen only for the film grown on a  $\text{SrLaAlO}_4$  (SLAO) substrate, which applied the in-plane compressive stress to the film. Such a  $\rho(T)$  anomaly is interpreted as a sign of the first-order phase transition related to the SS transition of Co ions, which was observed in the polycrystalline bulk. However, there has been no direct evidence of the cause of the  $\rho(T)$  anomaly, and no investigation of the thickness dependence of the  $\rho(T)$  anomaly has been attempted. Although the appearance of the MI transition with hysteresis and the increase in the transition temperature for the  $\text{Pr}_{1-x}\text{Ca}_x\text{CoO}_3$  bulk materials under hydrostatic pressure were reported previously,<sup>21,22</sup> the influence of the epitaxial stress due to lattice mismatch and the thermal stress due to the difference of thermal contraction coefficient between the film and substrate on the MI transition has not been clarified so far.

In the present work, we report on the PLD growth of 50–300 nm thick  $(\text{Pr}_{1-y}\text{Y}_y)_{1-x}\text{Ca}_x\text{CoO}_3$  epitaxial films on the SLAO substrate. To clarify the origin of the  $\rho(T)$  anomaly, the Pr  $L_2$ -edge XANES spectra and low-temperature magnetization are measured for the films. It appears that the valence change at Pr sites and the spin-state crossover of Co ions, known for polycrystalline samples, are realized also for the compressively strained thinner films, but the transition is of diffuse character and spreads over a wide temperature range. In thicker films showing different degrees of relaxation toward bulk  $(\text{Pr}_{1-y}\text{Y}_y)_{1-x}\text{Ca}_x\text{CoO}_3$  structure, the transition is inhibited. Absence of the transition is found also for films grown on the  $\text{LaAlO}_3$  (LAO) substrate that applies the in-plane tensile stress. These results suggest that substrates have generally a blocking effect, which prevents the films to accommodate  $\sim 1\%$  volume change below the transition to lower spin Co states, unless they are suitably strained at higher temperature or, eventually, possess structural defects with low-temperature mobility as reported elsewhere.<sup>33,35</sup>

## II. EXPERIMENTAL PROCEDURE

$(\text{Pr}_{1-y}\text{Y}_y)_{1-x}\text{Ca}_x\text{CoO}_3$  (PYCCO) thin films were fabricated by the PLD method using a fifth harmonic wave of Nd:YAG laser with  $\lambda = 213$  nm and a repetition rate of 10 Hz. The pulse duration was 5 ns and the power was 18 mJ. A polycrystalline target with nominal composition ( $x = 0.4$ ,  $y = 0.2$ ) was prepared by a standard solid-state reaction. The details of the fabrication method of the target bulk have been described elsewhere.<sup>34</sup> The target and the substrate were set in a PLD apparatus and were counter-rotated at a speed of 7 rpm and 3 rpm, respectively, to reduce non-uniform erosion

and to deposit the film uniformly. The deposition was carried out for 0.5–4 h in a pure oxygen pressure,  $P_{\text{O}_2} = 1.0$  Torr, and at a substrate temperature,  $T_s = 873$  K. The film thickness,  $d$ , was changed from 50 to 300 nm, which was determined by a contact profiler (Taylor Hobson Inc.). The films were grown on the (001) oriented SrLaAlO<sub>4</sub> (SLAO:  $a = 0.3756$  nm,  $c = 1.2636$  nm) single crystal substrate of 0.5 mm in thickness. For comparison, the films were also grown on the (001) oriented LaAlO<sub>3</sub> (LAO:  $a = 0.3790$  nm) single crystal substrate. The pseudo cubic lattice parameter of the PYCCO target bulk was  $a = 0.3775$  nm, and the lattice mismatch,  $\varepsilon = (a_{\text{film}} - a_{\text{sub}})/a_{\text{sub}}$ , was  $-0.5\%$  for SLAO and  $+0.4\%$  for LAO, where  $a_{\text{film}}$  and  $a_{\text{sub}}$  were lattice parameters of PYCCO film and substrate, respectively. In this case, an in-plane compressive stress was applied to the films grown on the SLAO substrate, and an in-plane tensile stress was applied to the films grown on the LAO substrate. The chemical composition of the grown films was estimated by electron probe microanalysis (EPMA), in which the composition of the  $(\text{Pr}_{1-y}\text{Y}_y)_{1-x}\text{Ca}_x\text{CoO}_3$  film was shifted to  $(x = 0.3, y = 0.125)$  from the nominal target composition of  $(x = 0.4, y = 0.2)$ . To clarify the crystalline quality of the grown films, X-ray diffraction analyses of a  $\theta/2\theta$  scan were performed using Cu  $K\alpha$  radiation, which identified the out-of-plane alignment. The electrical resistivity,  $\rho(T)$ , was measured on cooling and heating runs in the 10–300 K range by a standard four-probe method. In addition, test measurements of both the electrical resistivity and thermoelectric power were performed under flowing oxygen at room and high temperatures, and the results were compared with data for bulk  $(\text{Pr}_{1-y}\text{Y}_y)_{0.7}\text{Ca}_{0.3}\text{CoO}_3$  and  $\text{Pr}_{1-x}\text{Ca}_x\text{CoO}_3$  systems. Making use of well-known sensitivity of thermoelectric power to the cobalt oxidation state and thus to oxygen stoichiometry,<sup>36</sup> the close-to-ideal oxygen stoichiometry of present films was confirmed.

The temperature dependence of XANES spectra at the Pr  $L_2$ -edge was measured for the films at BL01B1 of SPring-8 in Japan. Because of the overlap of the fine structure of La  $L_2$ -edge from the substrate with the Pr  $L_3$ -edge from the film, we selected to measure the Pr  $L_2$ -edge XANES spectra, although we usually measured Pr  $L_3$ -edge XANES spectra in the bulk samples.<sup>27,30</sup> The X-ray beam was monochromatized using a Si(111) double-crystal monochromator. The spectra were recorded in the fluorescence mode by 19-ch solid-state detector (SSD) at various temperatures from 300 to 8 K using a cryocooler. The valence of all the Pr ions was supposed to be  $3.0+$  for all the films around room temperature. To determine the mixed  $\text{Pr}^{3+}/\text{Pr}^{4+}$  content in the film at low temperatures, comparative XANES measurements for  $\text{Pr}_6\text{O}_{11}$  ( $\text{Pr}^{3.667+}$ ) and  $\text{Pr}_2\text{O}_3$  ( $\text{Pr}^{3.0+}$ ) were also carried out. The recorded spectra were modeled by the sum of three Lorentzian functions and one arctangent function representing the step-like edge of the continuum excitations, similarly to the previous analyses.<sup>27,30</sup> One Lorentzian function (peak A: 6442 eV) shows a fluorescence from  $L_2$  ( $2p_{1/2}$ ) to  $M_4$ , which represents  $\text{Pr}^{3+}$  ions. The other Lorentzian functions (peak B2: 6445 eV and peak B1: 6455 eV) show the excitations from  $2p_{3/2}$  to  $4f^2\bar{L}5d^*$  and  $4f^1\bar{L}5d^*$ , with  $L$  being a ligand hole in the O  $2p$  orbital, both of which can be understood to

represent  $\text{Pr}^{4+}$  ions.<sup>37,38</sup> The energy differences between peaks A, B2, and B1 were fixed according to results of Hu *et al.*<sup>39</sup> The curve fittings were performed using Athena software.<sup>40</sup>

The magnetic properties were probed on the films of  $d = 160$  nm in thickness, by using a SQUID magnetometer. The susceptibility data were taken in the 2–300 K range, using the zero-field-cooled (ZFC) and field-cooled (FC) regimes and DC field of 10 kOe. The hysteresis loops up to 70 kOe were also scanned at 2 K. Moreover, in order to distinguish the magnetic response of the film from that of the substrate, careful chemical analysis of magnetic impurities in the SLAO and LAO substrates was performed.

### III. EXPERIMENTAL RESULTS AND DISCUSSION

#### A. Thickness dependence of the electrical resistivity, $\rho(T)$ , of PYCCO films on SLAO and LAO substrates

Figure 1(a) shows the thickness dependence of the electrical resistivity,  $\rho(T)$ , of PYCCO films ( $x = 0.3, y = 0.125$ ) with different thicknesses, grown on the SLAO substrate. The  $\rho(T)$  of the polycrystalline bulk with the same composition is also shown in the figure, which shows an abrupt jump of about two orders of magnitude at  $T_{\text{MI}} = 120$  K on the cooling run, and shows only very small hysteresis on heating run. In the PYCCO films, there is an anomalous upturn in the

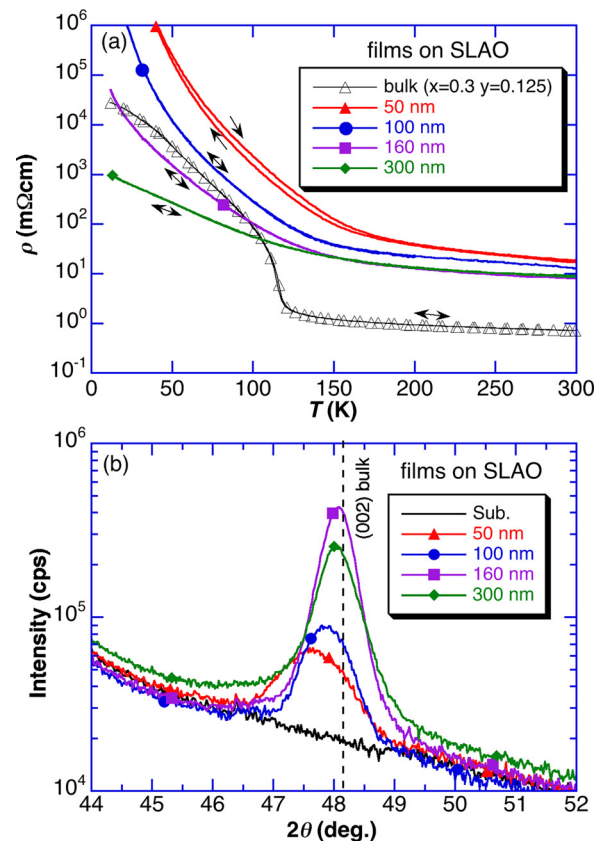


FIG. 1. (a) Thickness dependence of the electrical resistivity,  $\rho(T)$ , of the  $(\text{Pr}_{1-y}\text{Y}_y)_{1-x}\text{Ca}_x\text{CoO}_3$  ( $x = 0.3, y = 0.125$ ) epitaxial films grown on the SLAO substrate.  $\rho(T)$  of the polycrystalline bulk with the same composition is also shown. (b) Out-of-plane XRD patterns of the (002) diffraction for the same PYCCO films grown on the SLAO substrate.

$\rho(T)$  curve having an inflection at around 170 K and by broad hysteresis spreading to much lower temperatures that can be seen, however, for the film of  $d = 50$  nm only. For the films thicker than  $d = 100$  nm, the inflection in  $\rho(T)$  decreases with increasing film thickness,  $d$ , and no hysteresis can be distinguished.

Figure 1(b) presents the out-of-plane XRD patterns of the (002) diffraction for the same films. The peak intensity and the peak angle increased with increasing film thickness,  $d$ . The full width at half maximum (FWHM) value also decreased with increasing  $d$ , which was  $1.40^\circ$  for  $d = 50$  nm and  $1.07^\circ$  for  $d = 300$  nm, respectively. These results indicate that the 50 nm film is elastically compressed on the SLAO substrate, and this property is likely the reason for the observed hysteresis in the resistivity measurement. On the other hand, a partial relaxation takes place with increasing film thickness, for which the average lattice parameter of the  $c$ -axis approaches that of the bulk crystal and the epitaxial strain becomes effective only close to the interface.

Figure 2 shows the thickness dependence of the  $\rho(T)$  of PYCCO films ( $x = 0.3$ ,  $y = 0.125$ ) with different thicknesses grown on the LAO substrate. For all these films,  $\rho(T)$  slightly increases with decreasing temperature, which is a clear contrast to the notable upturn in PYCCO films on the SLAO substrate. No anomaly in  $\rho(T)$  can be detected, even for the films as thin as  $d = 100$  nm. And the absolute value of  $\rho(T)$  decreases with increasing film thickness,  $d$ .

## B. XANES spectra

Figure 3(a) shows the temperature dependence of the XANES spectra at the Pr  $L_2$ -edge for the  $d = 50$  nm film grown on the SLAO substrate. The two main peaks situated at 6442 and 6455 eV (named peaks A and B1) originate from the Pr  $L_2$  to  $M_4$  transitions. At 290 K, Pr<sup>3+</sup> sites essentially contribute to the peak A, with a little bump around 6455 eV caused presumably by multiple scattering, which is commonly introduced in the theoretical calculation of XANES.<sup>29</sup> The small bump was also observed at the Pr  $L_3$ -edge in the Pr<sub>2</sub>O<sub>3</sub> and Pr<sub>0.7</sub>Ca<sub>0.3</sub>CoO<sub>3</sub> polycrystals,<sup>27</sup> which is not related to the valence change of Pr ions. When the

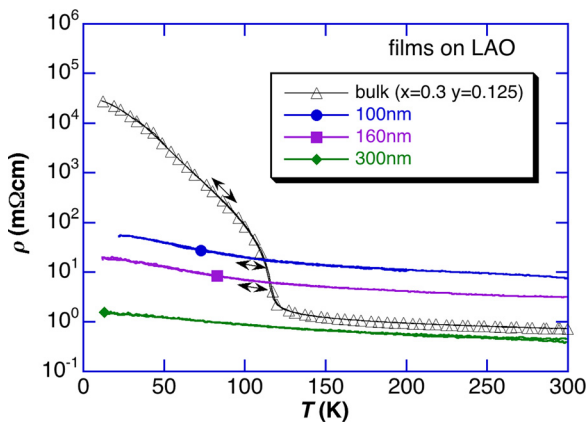


FIG. 2. Thickness dependence of the electrical resistivity,  $\rho(T)$ , of the  $(\text{Pr}_{1-y}\text{Y}_y)_{1-x}\text{Ca}_x\text{CoO}_3$  ( $x = 0.3$ ,  $y = 0.125$ ) epitaxial films grown on the LAO substrate.  $\rho(T)$  of the polycrystalline bulk with the same composition is also shown.

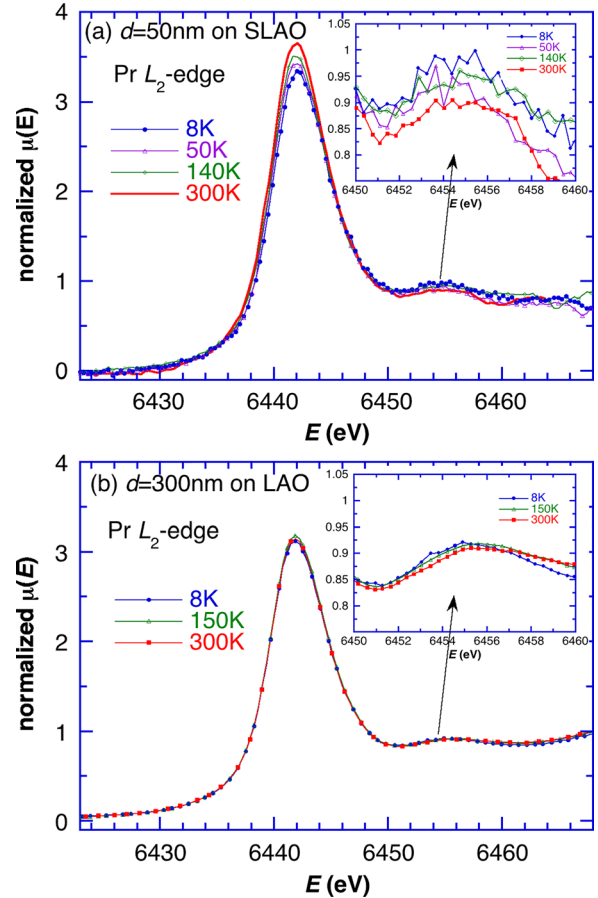


FIG. 3. Temperature dependence of the XANES spectra at the Pr  $L_2$ -edge for the (a)  $d = 50$  nm film grown on the SLAO substrate and (b)  $d = 300$  nm film grown on the LAO substrate. The inset of each figure shows the magnification of the spectra around 6455 eV.

temperature decreases, the shape of the XANES spectra changes markedly. The intensity of peak B1 slightly increases and, at the same time, the intensity of peak A decreases and a new component (peak B2 at 6445 eV) can be resolved on its high-energy slope. The B1 and B2 peaks are manifestations of Pr<sup>4+</sup> states.<sup>37–39</sup> These results suggest that, for the  $d = 50$  nm film, the valence of the Pr ions increases from 3+ toward 4+ with decreasing temperature, which is consistent with the reports for the PYCCO and Pr<sub>0.5</sub>Ca<sub>0.5</sub>CoO<sub>3</sub> polycrystals.<sup>29,30,41</sup>

Figure 3(b) shows the temperature dependence of the XANES spectra at the Pr  $L_2$ -edge for the  $d = 300$  nm film grown on the LAO substrate. Because of the strong signal from the thicker film, the spectra are not noisy compared with those for the  $d = 50$  nm film shown in Fig. 3(a). Apart from the main peak A, there is again a small bump at around 6455 eV, originating in the multiple scattering as mentioned above. The intensities of peaks A and B1 are almost the same, even if the temperature decreases down to 8 K, which suggests that the valence of the Pr ions is almost constant of 3.0+ at the entire temperature range.

In order to determine the valence shift quantitatively, the XANES spectra were fitted to a sum of three Lorentzian functions (peak A for Pr<sup>3+</sup> and peaks B1 and B2 for Pr<sup>4+</sup>) and one arctangent function representing the continuum excitations, as indicated in Section II. Figures 4(a) and 4(b)

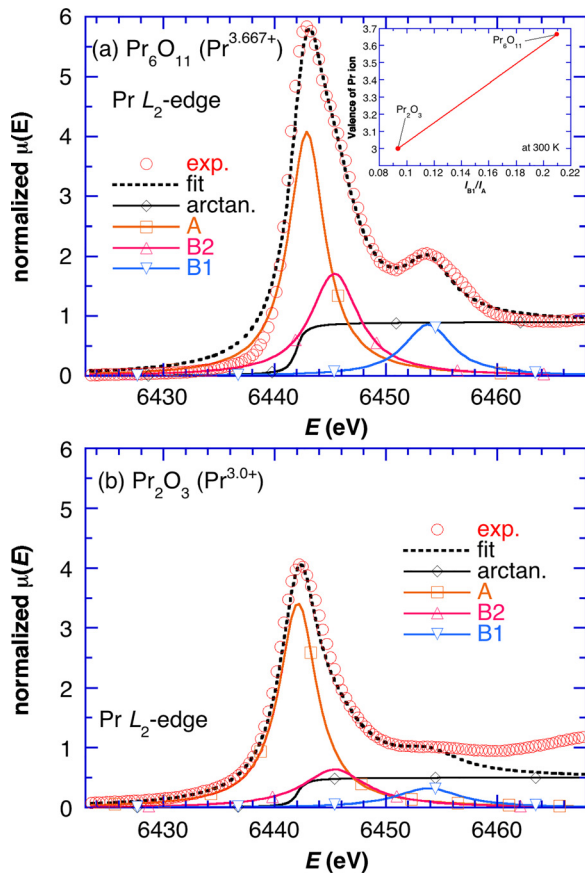


FIG. 4. XANES spectrum at the Pr  $L_2$ -edge of the (a)  $\text{Pr}_6\text{O}_{11}$  and (b)  $\text{Pr}_2\text{O}_3$  samples at 300 K, for which the fitting was performed. The inset in (a) shows the calibration line for the determination of the valence of the Pr ion in the films used in the study.

show the XANES spectrum at the Pr  $L_2$ -edge of  $\text{Pr}_6\text{O}_{11}$  and  $\text{Pr}_2\text{O}_3$  at 300 K, which are, respectively, regarded as a standard for  $\text{Pr}^{3.667+}$  and  $\text{Pr}^{3.0+}$ . In the fitting of the temperature-dependent XANES spectra for the PYCCO films, the intensity ratio of B1:B2 was fixed to be 1.0:2.0. The calibration line was used for the determination of the valence of the Pr ion shown in the inset of Fig. 4(a).

Figure 5(a) shows an example of the fitting curve of the XANES spectrum at 8 K for the  $d=50$  nm film grown on the SLAO substrate, where the valence change achieves a maximum. It is seen that the XANES spectrum can be well fitted within the energy range including the related peaks of  $\text{Pr}^{3+}$  and  $\text{Pr}^{4+}$ . The B2 component is also resolved and appears notable so that the resemblance with the  $\text{Pr}^{3+}/\text{Pr}^{4+}$  mixture in  $\text{Pr}_6\text{O}_{11}$  is obvious. The temperature course of the valence of the Pr ion is shown in Fig. 5(b) for the films. For the  $d=50$  nm film on the SLAO substrate, the average Pr valence increases gradually on cooling from 300 K, and reaches a final value of 3.15+ at 8 K. It is worth mentioning that in our previous study of the  $(\text{Pr}_{1-y}\text{Y}_y)_{0.7}\text{Ca}_{0.3}\text{CoO}_3$  bulk materials, the Pr valence varied from 3.15+ in  $y=0.075$  up to 3.27+ in  $y=0.15$  at 8 K.<sup>27</sup> The Pr valence of 3.15+ for the present  $d=50$  nm film ( $x=0.3$ ,  $y=0.125$ ) on the SLAO substrate is lower than expected for bulk material of this composition, 3.23+. This may signal that the in-plane compressive strain, which is the driving force for low-temperature transition

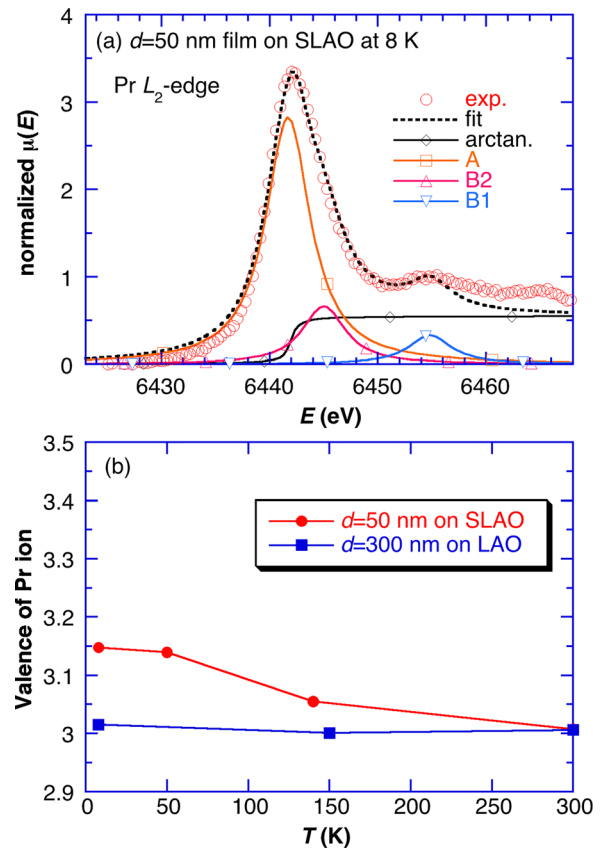


FIG. 5. (a) Example of the fitting of the XANES spectrum at 8 K for the  $d=50$  nm film on the SLAO substrate. For the fitting, one arctangent function and three Lorentzian functions are used. (b) Temperature dependence of the valence of Pr ions in the films ( $d=50$  nm on SLAO and  $d=300$  nm on LAO) estimated using the XANES spectra and curve fitting.

in PYCCO epitaxial films, was exhausted before the transition could be completed. On the other hand, for the  $d=300$  nm film on the LAO, there was no change in the valence of the Pr ion down to 8 K, which suggested that the valence of the Pr ion remained at 3.0+. The ambiguity of the estimated valence values is  $\sim 0.03$ , which results from the arbitrariness of the parameters in the arctangent and Lorentzian functions used. The XANES spectra thus provide strong arguments that the  $\rho(T)$  anomaly for the  $d=50$  nm film on the SLAO substrate results from the spin-state (SS) transition of Co ions, similar to the PYCCO polycrystalline bulks.

### C. Magnetization of PYCCO films on SLAO and LAO substrates

The magnetic behavior was investigated for the thick  $(\text{Pr}_{1-y}\text{Y}_y)_{1-x}\text{Ca}_x\text{CoO}_3$  ( $x=0.3$ ,  $y=0.125$ ) films ( $d=160$  nm) grown on the SLAO and LAO substrates at  $T_s=873$  K and  $P_{\text{O}_2}=0.01$  Torr for 1 h. Although it is the best to measure the same films ( $d=50$  nm film on SLAO and  $d=300$  nm film on LAO) as shown in Fig. 3, the thicker films must be measured to enhance the intrinsic magnetic signal of the films. Because a single crystal SLAO substrate grown in an iridium (Ir) crucible contained the minute contamination of  $\text{Ir}^{4+}$  species with magnetic moment,  $j=1/2$ , which affect to the low temperature paramagnetic tail superposed to the dominant diamagnetic response of the PYCCO film. For this

reason, the thicker  $d = 160$  nm films were used for the magnetic investigation. Figure 6(a) shows the temperature dependence of the magnetic susceptibility  $\chi(T)$  of the films during field cooling (FC) and zero-field cooling (ZFC) runs under the magnetic field of  $\mu_0 H = 10$  kOe. For comparison, the same  $\chi(T)$  plots for the reference bulk samples are shown in Fig. 6(b), in which the PYCCO bulk ( $x = 0.3$ ,  $y = 0.15$ ), abbreviated as “PrY15,” exhibits a clear MI transition characterized by a sharp drop of magnetic susceptibility at 134 K,<sup>26</sup> and the pure  $\text{Pr}_{0.7}\text{Ca}_{0.3}\text{CoO}_3$  bulk, abbreviated as “PrCa30,” does not undergo any MI-SS transition and shows instead a marked upturn of susceptibility at  $\sim 80$  K, which signals the

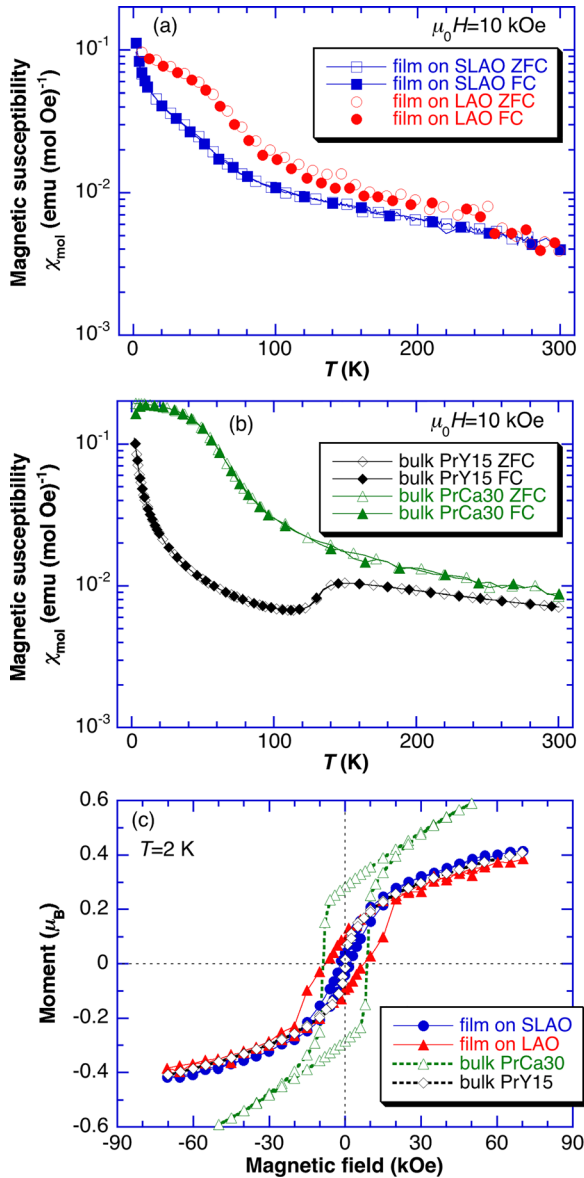


FIG. 6. (a) The ZFC/FC susceptibility curves of the  $(\text{Pr}_{1-y}\text{Y}_y)_{1-x}\text{Ca}_x\text{CoO}_3$  ( $x = 0.3$ ,  $y = 0.125$ ) epitaxial films 160 nm in thickness, grown on the SLAO and LAO substrates. The measurement was done at 10 kOe. (b) The similar ZFC/FC susceptibility curves of the  $(\text{Pr}_{1-y}\text{Y}_y)_{1-x}\text{Ca}_x\text{CoO}_3$  bulks ( $x = 0.3$ ,  $y = 0.15$ ; “PrY15” and  $x = 0.3$ ,  $y = 0$ ; “PrCa30”) referred from Ref. 26, which are examples of the presence and absence of MI transition, respectively. (c) The hysteresis loops of the films at 2 K. Diamagnetic contribution of both substrates together with low temperature paramagnetism associated with magnetic impurities in case of SLAO substrate were subtracted (see text).

spontaneous FM ordering at  $T_c = 55$  K.<sup>26,42</sup> Figure 6(c) shows the magnetization loops measured at 2 K for the films, compared with the PrY15 and PrCa30 bulks. It should be noted that the magnetic data on the present PYCCO films are subjected to a large uncertainty due to small intrinsic signals of the layer itself, superimposed to the paramagnetic contribution of substrates. The eventual inaccuracy in the film thickness determination and, importantly, certain paramagnetic contamination of Ir in the SLAO substrate that are of the Curie-type temperature dependence and interfere thus with diamagnetism of the films, further complicates the quantitative analysis.<sup>43</sup>

Nonetheless, in spite of these limitations, we would like to note that the ZFC/FC susceptibility curves observed for PYCCO/SLAO film remind the Curie-type behavior of the PrY15 bulk, although a reduction of magnetic susceptibility cannot be observed, which may come from the diffuse character of MI transition. However, the narrow hysteresis loop at 2 K is of a similar curvature and magnitude as found in the PrY15 bulk with similar chemical composition undergoing the MI transition. Even for the moderate MI transition in the PYCCO/SLAO film ( $d = 160$  nm), we can unambiguously exclude the persistence of the metallic phase down to low temperatures. We deduce that the dominant part of  $\text{Co}^{3+}$  ions in the PYCCO film grown on SLAO substrate with a small negative mismatch  $\varepsilon = -0.5\%$  occurs likely in the LS state, which is an essential characteristic of the insulating state.

On the other hand, the magnetic properties of PYCCO/LAO film with  $\varepsilon = +0.4\%$  are distinct both by the presence of FM upturn in ZFC/FC susceptibility curves below  $\sim 80$  K and by a large coercivity in hysteresis loop at 2 K. The magnetization curve remarkably resembles the results on  $\text{Pr}_{0.7}\text{Ca}_{0.3}\text{CoO}_3$  bulk, though the absolute value of the remnant moment is reduced (see Fig. 6(c)). Magnetic characterization (not shown) of the PYCCO film grown on  $\text{SrTiO}_3$  (STO) substrate with the largest mismatch of  $\varepsilon = +3.4\%$  have shown that ZFC/FC susceptibility curves exhibit similar FM upturn as PYCCO/LAO film and large coercivity in hysteresis loop at 2 K as well. Moreover, the low temperature remnant moment was even higher than that detected in the PYCCO/LAO films. We thus conclude that PYCCO film grown on substrates with a positive mismatch retains the ferromagnetic metallic phase of  $t_{2g}^5\sigma^*$  character with delocalized carriers in the antibonding  $e_g$  band down to the lowest temperatures.

#### IV. DISCUSSION

In the bulk  $(\text{Pr}_{1-x}\text{RE}_y)_{1-x}\text{Ca}_x\text{CoO}_3$  systems under ambient pressure, which show the simultaneous MI-SS transition, a volume contraction of  $\sim 1\%$  took place below  $T_{MI} \sim 100$  K.<sup>44</sup> The entropy change makes  $\Delta S \sim 5 \text{ J}\cdot\text{K}^{-1}\cdot\text{mol}^{-1}$ ,<sup>45,46</sup> which means that the internal energy of the low-temperature phase is about  $\Delta S \cdot T_{MI} \sim 500 \text{ J}\cdot\text{mol}^{-1}$  lower, compared with the high-temperature phase. The present PYCCO films are fixed on the substrate and the lattice parameters and the unit cell volume are difficult to change. Even if a suitable condition for the MI-SS transition were obtained, it would be at some

expense of elastic energy due to strains that are frozen at low temperatures.

In the PYCCO films on SLAO, the lattice mismatch,  $\varepsilon = -0.5\%$ , exists at room temperature and thermal stress is also applied to the films during low temperature  $\rho(T)$  measurements, which results from the difference of thermal contraction coefficient between the PYCCO film and SLAO substrate. Since the thermal contraction coefficient of PYCCO is about twice as large as that of the SLAO substrate,<sup>47,48</sup> the lattice mismatch is effectively decreased at low temperatures, to about  $\varepsilon = -0.25\%$  at 50 K. The in-plane stress, which is exerted on the film, can be roughly estimated by  $\sigma = \varepsilon \cdot Y \cdot (1 - \nu)^{-1}$  with  $Y$  and  $\nu$  being the Young modulus and the Poisson ratio, respectively.<sup>48,49</sup> Assuming for cobaltites,  $Y = 150 \text{ GPa}$ <sup>50</sup> and  $\nu = 0.3$ ,<sup>51</sup> we arrive to the conclusion that the compressive in-plane stress makes  $\sigma_e = -1.07 \text{ GPa}$  at 300 K and  $\sigma_e + \sigma_t = -0.535 \text{ GPa}$  at 50 K, which is a favorable condition to start the MI-SS transition in PYCCO even at higher temperatures than in polycrystalline bulks. However, this compressive strain is gradually spent since the complete transition to the low-temperature state is characterized by rather large volume contraction of  $\sim 1\%$ , which would make an additional in-plane strain of tensile character,  $\varepsilon_{MI} = +0.33\%$ . The corresponding in-plane tensile stress  $\sigma_{MI} = +0.715 \text{ GPa}$  thus cancels the compressive in-plane stress  $\sigma_e + \sigma_t = -0.535 \text{ GPa}$  that exists in the high-temperature phase.

In the case of thick PYCCO films that can be considered as nearly relaxed at room temperature, the different thermal contraction between the film and substrate brings a tensile in-plane stress at low temperatures,  $\sigma_t = +0.535 \text{ GPa}$  at 50 K, which would be increased, upon the MI-SS transition to  $\sigma_t + \sigma_{MI} = 1.250 \text{ GPa}$  as derived from the strain ( $\varepsilon + \varepsilon_{MI} = +0.58\%$ ). Neglecting the inhomogeneities close to the substrate–film interface, the corresponding elastic energy of uniformly strained films (per unit volume) can be written as  $E = 1/2(\sigma_{11} \cdot \varepsilon_{11} + \sigma_{22} \cdot \varepsilon_{22})$  with only in-plane variables  $\sigma_{11} = \sigma_{22}$  and  $\varepsilon_{11} = \varepsilon_{22}$ , while the other terms become zero either because of the absence of shear strain ( $\varepsilon_{12} = 0$ ) or because of the absence of out-of-plane stress ( $\sigma_{33} = 0$ ). For  $\sigma_t + \sigma_{MI} = 1.250 \text{ GPa}$ ,  $\varepsilon_t + \varepsilon_{MI} = +0.58\%$  and actual molar volume, the formula gives an estimate that the elastic energy accumulated during the MI-SS transition might be as high as  $E = 950 \text{ J} \cdot \text{mol}^{-1}$ . Although this value might be partly reduced at the presence of defects, it is clear that the rise of energy due to frozen strains exceeds or is at least comparable to the above mentioned drop of energy,  $\Delta S \cdot T_{MI} \sim 500 \text{ J} \cdot \text{mol}^{-1}$ . In other words, there is no driving force for MI-SS transition in relaxed PYCCO films.

We conclude that the discussed elastic properties may explain well what is actually observed, namely the diffuse character of MI-SS transition in compressively strained 50 nm thick PYCCO film on SLAO substrate and the absence of transition in thicker relaxed films or thin tensile-strained films.

## V. SUMMARY

$(\text{Pr}_{1-y}\text{Y}_y)_{1-x}\text{Ca}_x\text{CoO}_3$  (PYCCO) epitaxial films, with hole doping controlled by the calcium content  $x = 0.3$  and

structurally modified by content of small size yttrium  $y = 0.125$ , have been fabricated by the pulsed laser deposition (PLD) method on the  $\text{SrLaAlO}_4$  (SLAO) and  $\text{LaAlO}_3$  (LAO) single crystal substrates. The thickness dependence of electrical resistivity,  $\rho(T)$ , has been investigated and the compressive stress of the films on the SLAO substrate has been analyzed. The most important results and conclusions are summarized as follows:

- (1) An anomalous  $\rho(T)$  upturn with wide hysteresis can be clearly observed only for the thinnest film ( $d = 50 \text{ nm}$ ) grown on the SLAO substrate. The hysteretic  $\rho(T)$  anomaly vanished for the films thicker than  $d = 100 \text{ nm}$  and inflections in  $\rho(T)$  around 170 K decreased with increasing film thickness,  $d$ . These results indicate a gradual loss of the full compressive stress with increasing  $d$ .
- (2) On the other hand, the  $\rho(T)$  of the film grown on the LAO substrate, which applied the tensile stress to the film, shows no anomaly, and the absolute value of  $\rho(T)$  decreases with increasing the film thickness,  $d$ .
- (3) From the measurements of the XANES spectra at the Pr  $L_2$  for the films, the average valence of the Pr ion in the  $d = 50 \text{ nm}$  film on the SLAO substrate slightly increases with decreasing temperature from the common value 3.0+ at around room temperature to 3.15+ at 8 K. On the other hand, there is no valence shift of Pr in the film on the LAO substrate in the entire temperature range. These results strongly suggest that the anomalous  $\rho(T)$  upturn in the thin film on the SLAO substrate is closely related to the MI-SS transition seen in PYCCO polycrystalline bulks.
- (4) The Curie-type susceptibility  $\chi(T)$  curve and the narrow hysteresis loop at 2 K in the PYCCO thin film grown on SLAO substrate are the similar trends to the PYCCO bulk with MI transition. These results suggest an essential characteristic behavior of the insulating state at low temperatures, in which LS  $\text{Co}^{3+}$  ionic states dominate. On the other hand, PYCCO films grown on LAO substrate retain the ferromagnetic metallic phase of  $t_{2g}^5 \sigma^*$  character with delocalized carriers in the antibonding  $e_g$  band down to the lowest temperatures.
- (5) The strain exerted by substrates on epitaxial films hinders to develop volume change required for the low-temperature spin-state transition. The epitaxial compressive strain is gradually spent during the transition, so that the remaining regions of the high temperature state will need lower and lower temperatures to transform into the low temperature state. Therefore, the transition in the epitaxial thin film on SLAO is diffuse and spreads over a large temperature range. On the other hand, thick films experience generally a tensile strain that increases with decreasing temperature. This is completely unfavorable situation since large elastic energy would be accumulated upon the MI-SS transition.

## ACKNOWLEDGMENTS

The synchrotron radiation experiments were performed at the BL01B1 of SPring-8 with approval of the Japan

Synchrotron Radiation Research Institute (JASRI) (Proposal Nos. 2013A1093 and 2016B1089). The authors thank Dr. T. Ina of JASRI for his experimental assistance for XRF measurements. This work was partly supported by JSPS KAKENHI (Grant No. 24540355) and was performed under the Inter-university Cooperative Research Program of the Institute for Materials Research, Tohoku University. The work at Institute of Physics, Prague, was supported by Project No. 17-04412S of the Czech Science Foundation.

- <sup>1</sup>P. M. Raccach and J. B. Goodenough, *Phys. Rev.* **155**, 932 (1967).
- <sup>2</sup>M. A. Korotin, S. Y. Ezhov, I. V. Solovyev, V. I. Anisimov, D. I. Khomskii, and G. A. Sawatzky, *Phys. Rev. B* **54**, 5309 (1996).
- <sup>3</sup>K. Asai, A. Yoneda, O. Yokokura, J. M. Tranquada, G. Shirane, and K. Kohn, *J. Phys. Soc. Jpn.* **67**, 290 (1998).
- <sup>4</sup>T. Kyomen, Y. Asaka, and M. Itoh, *Phys. Rev. B* **71**, 024418 (2005).
- <sup>5</sup>S. W. Biernacki, *Phys. Rev. B* **74**, 184420 (2006).
- <sup>6</sup>P. G. Radaelli and S.-W. Cheong, *Phys. Rev. B* **66**, 094408 (2002).
- <sup>7</sup>D. Phelan, D. Louca, S. Rosenkranz, S.-H. Lee, Y. Qui, P. J. Chupas, R. Osborn, H. Zheng, J. F. Michell, J. R. D. Copley, J. L. Sarrjo, and Y. Morimoto, *Phys. Rev. Lett.* **96**, 227201 (2006).
- <sup>8</sup>C. He, S. El-Khatib, J. Wu, J. W. Lynn, H. Zheng, J. F. Michell, and C. Leighton, *Eur. Lett.* **87**, 27006 (2009).
- <sup>9</sup>D. Phelan, D. Louca, K. Kamazawa, S.-H. Lee, S. N. Ancona, S. Rosenkranz, Y. Motome, M. F. Hundley, J. F. Michell, and Y. Morimoto, *Phys. Rev. Lett.* **97**, 235501 (2006).
- <sup>10</sup>H. M. Aarbogh, J. Wu, L. Wang, H. Zheng, J. F. Michell, and C. Leighton, *Phys. Rev. B* **74**, 134408 (2006).
- <sup>11</sup>M. Itoh, I. Natori, S. Kubota, and K. Motoya, *J. Phys. Soc. Jpn.* **63**, 1486 (1994).
- <sup>12</sup>D. N. Nam, K. Jonason, P. Nordblad, N. V. Khiem, and N. X. Phuc, *Phys. Rev. B* **59**, 4189 (1999).
- <sup>13</sup>P. L. Kuhns, M. J. R. Hoch, W. G. Moulton, A. P. Reyes, J. Wu, and C. Leighton, *Phys. Rev. Lett.* **91**, 127202 (2003).
- <sup>14</sup>K. Knizek, Z. Jirak, J. Hejtmanek, P. Novak, and W. Ku, *Phys. Rev. B* **79**, 014430 (2009).
- <sup>15</sup>V. Krapek, P. Novak, J. Kunes, D. Novoselov, Dm. M. Korotin, and V. I. Anisimov, *Phys. Rev. B* **86**, 195104 (2012).
- <sup>16</sup>Z. Jirak, J. Hejtmanek, K. Knizek, and M. Veverka, *Phys. Rev. B* **78**, 014432 (2008).
- <sup>17</sup>A. Doi, J. Fujioka, T. Fukuda, S. Tsutsui, D. Okuyama, Y. Taguchi, T. Arima, A. Q. R. Baron, and Y. Tokura, *Phys. Rev. B* **90**, 081109(R) (2014).
- <sup>18</sup>S. Tsubouchi, T. Kyömen, M. Itoh, P. Ganguly, M. Oguni, Y. Shimojo, Y. Morii, and Y. Ishii, *Phys. Rev. B* **66**, 052418 (2002).
- <sup>19</sup>S. Tsubouchi, T. Kyömen, M. Itoh, and M. Oguni, *Phys. Rev. B* **69**, 144406 (2004).
- <sup>20</sup>T. Saitoh, Y. Yamashita, N. Todoroki, T. Kyomen, M. Itoh, M. Higashiguchi, M. Nakatake, and K. Shimada, *J. Electron. Spectrosc. Relat. Phenom.* **144–147**, 893 (2005).
- <sup>21</sup>T. Fujita, T. Miyashita, Y. Yasui, Y. Kobayashi, M. Sato, E. Nishibori, M. Sakata, Y. Shimojo, N. Igawa, Y. Ishii, K. Kakurai, T. Adachi, Y. Ohishi, and M. Takata, *J. Phys. Soc. Jpn.* **73**, 1987 (2004).
- <sup>22</sup>T. Fujita, S. Kawabata, M. Sato, N. Kurita, M. Hedo, and Y. Uwatoko, *J. Phys. Soc. Jpn.* **74**, 2294 (2005).
- <sup>23</sup>T. Naito, H. Sasaki, and H. Fujishiro, *J. Phys. Soc. Jpn.* **79**, 034710 (2010).
- <sup>24</sup>T. Naito, H. Fujishiro, T. Nishizaki, N. Kobayashi, J. Hejtmanek, K. Knizek, and Z. Jirak, *J. Appl. Phys.* **115**, 233914 (2014).
- <sup>25</sup>K. Knizek, J. Hejtmanek, P. Novak, and Z. Jirak, *Phys. Rev. B* **81**, 155113 (2010).
- <sup>26</sup>J. Hejtmanek, E. Santava, K. Knizek, M. Marysko, Z. Jirak, T. Naito, H. Sasaki, and H. Fujishiro, *Phys. Rev. B* **82**, 165107 (2010).
- <sup>27</sup>H. Fujishiro, T. Naito, S. Ogawa, N. Yoshida, K. Nitta, J. Hejtmanek, K. Knizek, and Z. Jirak, *J. Phys. Soc. Jpn.* **81**, 064709 (2012).
- <sup>28</sup>J. L. Garcia-Munoz, C. Frontera, A. J. Baron-Gonzalez, S. Valencia, J. Blasco, R. Feyerherm, E. Dudzik, R. Abrudan, and F. Radu, *Phys. Rev. B* **84**, 045104 (2011).
- <sup>29</sup>J. Herrero-Martín, J. L. Garcia-Munoz, S. Valencia, C. Frontera, J. Blasco, A. J. Baron-Gonzalez, G. Subias, R. Abrudan, F. Radu, E. Dudzik, and R. Feyerherm, *Phys. Rev. B* **84**, 115131 (2011).
- <sup>30</sup>H. Fujishiro, T. Naito, D. Takeda, N. Yoshida, T. Watanabe, K. Nitta, J. Hejtmanek, K. Knizek, and Z. Jirak, *Phys. Rev. B* **87**, 155153 (2013).
- <sup>31</sup>D. Phelan, K. P. Bhatti, M. Taylor, S. Wang, and C. Leighton, *Phys. Rev. B* **89**, 184427 (2014).
- <sup>32</sup>M. Kriener, C. Zobel, A. Reichl, J. Baier, M. Cwik, K. Berggold, H. Kierspel, O. Zabara, A. Freimuth, and T. Lorenz, *Phys. Rev. B* **69**, 094417 (2004).
- <sup>33</sup>V. V. Mehta, N. Biskup, C. Jenkins, E. Arenholz, M. Varela, and Y. Suzuki, *Phys. Rev. B* **91**, 144418 (2015).
- <sup>34</sup>Y. Noda, H. Fujishiro, T. Naito, A. Ito, T. Goto, J. Hejtmanek, and Z. Jirak, *AIP Adv.* **6**, 025318 (2016).
- <sup>35</sup>A. Gulec, D. Phelan, C. Leighton, and R. F. Klie, *ACS Nano* **10**, 938 (2016).
- <sup>36</sup>Y. Wang, Y. Sui, P. Ren, L. Wang, X. Wang, W. Su, and H. J. Fan, *Inorg. Chem.* **49**, 3216 (2010).
- <sup>37</sup>H. Yamaoka, H. Oohashi, I. Jarrige, T. Terashima, Y. Zou, H. Mizota, S. Sakakura, T. Tochio, Y. Ito, E. Ya. Sherman, and A. Kotani, *Phys. Rev. B* **77**, 045135 (2008).
- <sup>38</sup>A. Bianconi, A. Kotani, K. Okada, R. Giorgi, A. Gargano, A. Marcelli, and T. Miyahara, *Phys. Rev. B* **35**, 806 (1987).
- <sup>39</sup>Z. Hu, S. Bertram, and G. Kaindl, *Phys. Rev. B* **49**, 39 (1994).
- <sup>40</sup>B. Ravel and M. Newville, *J. Synchrotron Radiat.* **12**, 537 (2005).
- <sup>41</sup>J. Hejtmanek, Z. Jirak, O. Kaman, K. Knizek, E. Santava, K. Nitta, T. Naito, and H. Fujishiro, *Eur. Phys. J. B* **86**, 305 (2013).
- <sup>42</sup>Z. Jirak, J. Hejtmanek, K. Knizek, M. Marysko, P. Novak, E. Santava, T. Naito, and H. Fujishiro, *J. Phys. Condens. Matter* **25**, 216006 (2013).
- <sup>43</sup>E. Talik, A. Pajaczkowska, A. Guzik, P. Zajdel, J. Kusz, A. Klos, and A. Szysiak, *Mater. Sci. Eng. B* **182**, 74 (2014).
- <sup>44</sup>K. Knizek, J. Hejtmanek, M. Marysko, P. Novak, E. Santava, Z. Jirak, T. Naito, and H. Fujishiro, *Phys. Rev. B* **88**, 224412 (2013).
- <sup>45</sup>M. Marysko, Z. Jirak, K. Knizek, P. Novak, J. Hejtmanek, T. Naito, H. Sasaki, and H. Fujishiro, *J. Appl. Phys.* **109**, 07E127 (2011).
- <sup>46</sup>V. Hardy, F. Guillou, and Y. Breard, *J. Phys.: Condens. Matter* **25**, 246003 (2013).
- <sup>47</sup>T. Naito, H. Sasaki, H. Fujishiro, and M. Yoshizawa, *J. Phys. Conf. Ser.* **200**, 012137 (2010).
- <sup>48</sup>D. Fuchs, E. Arac, C. Pinta, S. Schuppler, R. Schneider, and H. V. Löhneysen, *Phys. Rev. B* **77**, 014434 (2008).
- <sup>49</sup>A. H. Cottrell, in *The Mechanical Properties of Matter* (John Wiley and Sons, Inc., New York-London-Sydney, 1964), pp. 115 and 136.
- <sup>50</sup>T. Vogt, J. A. Hriljac, N. C. Hyatt, and P. Woodward, *Phys. Rev. B* **67**, 140401(R) (2003).
- <sup>51</sup>N. Orlovskaya, K. Kleveland, T. Grande, and M. A. Einarsrud, *J. Eur. Ceram. Soc.* **20**, 51 (2000).